Comparative Analysis of Empirical Models for Estimating Global Solar Radiation in Biratnagar, Nepal: A Case Study Using RadEst 3.0

Basanta Kumar Rajbanshi¹, Ram Gopal Singh², Kishor Khatiwada³, Anil Thapa³, Bed Raj KC⁴

¹Research Scholar, Shri Ramswaroop Memorial University (SRMU), Lucknow, India, basantaraz22@gmail.com

²Dean, Faculty of Physical Sciences, Shri Ramswaroop Memorial University (SRMU), Lucknow, India

³Research Scholar, St. Xavier's College, Kathmandu, Nepal ⁴Vice Chancellor, Pokhara University, Nepal

A detailed understanding of the geographic distribution of solar radiation is critical for advancing solar energy technologies. This study estimated the daily Global Solar Radiation (GSR) for Biratnagar, Nepal (26.48°N, 87.26°E, 75 m) for the years 2020-2023 using seven meteorological parameters: maximum and minimum temperatures, precipitation, solar radiation, maximum and minimum humidity, and wind speed. RadEst 3.0 was employed for these estimations.

Four models; Bristow and Campbell (BC), Campbell and Donatelli (CD), Donatelli and Bellocchi (DB), and a combined Donatelli-Campbell-Bristow-Bellocchi (DCBB) were applied to calculate GSR. Their performance was evaluated using statistical metrics, including the coefficient of determination (R²), mean bias error (MBE), mean percentage error (MPE), and root mean square error (RMSE). Parameter fitting (PF) was conducted to improve model accuracy by maximizing R² and minimizing CRM and RMSE.

The annual average GSR values for 2020, 2022, and 2023 were 14.7 \pm 0.30 MJ/m²/day, 15.4 \pm 0.25 MJ/m²/day, and 14.8 \pm 0.30 MJ/m²/day, respectively. The highest GSR value, 29.6 MJ/m²/day, was recorded in 2022, with a total yearly GSR of 5634 MJ/m². Among the models, the DCBB model consistently demonstrated the highest R² values across all three years, establishing it as the most reliable model for estimating GSR in this region.

1. Introduction

Nepal, known for its diverse topography, features mountains of varying elevations that contribute to its unique geomorphology. Positioned within the solar energy-friendly belt globally, the country covers an area of 147,516 km2, stretching approximately 800 km in length and 200 km in width. Located between 80°4' to 88°12' E longitude and 26°22' to 30°27' N latitude, Nepal is a landlocked nation sharing borders with India and China. Its climate and biodiversity vary exceptionally, shifting weather patterns every 200 m altitude. Due to the absence of domestic fossil fuel resources, including natural gas, coal and oil, Nepal faces significant energy shortages, which have hindered its economic and social progress.

The Alternative Energy Promotion Centre (AEPC), through its Solar and Wind Energy Resource Assessment (SWERA) initiative, has determined that Nepal has the potential to economically install up to 2,100 MW of on-grid solar PV systems. By 2022, approximately 974,000 residential solar PV systems had been deployed, primarily in the remote areas of Western Nepal where access to grid electricity remains highly limited. (WECS, Energy Synopsis Report, 2023)

During the fiscal year 2017/18, 2.2% of total energy consumption was derived from renewable sources, 27.8% from traditional sources, and 70% from commercial sources. Firewood remains the most widely used traditional energy source, but its inefficient use leads to forest depletion and poses health risks due to indoor air pollution from open fireplaces. According to Lamsal, 22% of the population remains without access to electricity, as power supply is primarily focused on urban regions. In the dry season, extended daily power outages significantly impact businesses, industries, and households. Furthermore, there is limited awareness among industries, businesses, and households about the economic and environmental advantages of energy efficiency. Standardizing energy-efficient products for households, lighting solutions, and industrial innovations remains insufficient.

In 2021, fuel sales saw a rise of 10.87%, with diesel increasing by 12.6%, kerosene by 21.61%, and LPG by 6.19%. Conversely, sales of Alternative Technology Fuels (ATF) experienced a sharp decline of 65.32%. In 2022, petrol sales surged by 40.43%, nearly quadrupling in value. Similarly, sales values for diesel, LPG, and ATF grew by 32.24%, 11.5%, and 74.55%, respectively. However, kerosene sales dropped by 4.99% during the same period. (WECS, Energy Synopsis Report, 2023)

Solar radiation represents a reliable and environmentally friendly energy resource. Nepal's average solar insolation varies between 3.6 and 6.2 kWh/m²/day annually. Shrestha et al. (2003) reported that the country experiences approximately 300 sunny days per year with an average of 6.8 hours of daily sunshine, highlighting the significant potential for harnessing free and sustainable solar energy. According to Poudyal (2015), the current annual average GSR is 4.23 kWh/m²/day. Consequently, solar energy serves as a critical and sustainable solution to address global energy demands, particularly in emerging economies like Nepal. (Joshi et. al. 2020)

Various formulas of varying complexity, including the standard Angstrom equation, can be employed to efficiently estimate GSR using recorded sunshine duration and other meteorological parameters. (Angstrom 1924; Iqbal 1983).

Olomiyesan et al. evaluated the performance of four methodologies to estimate GSR for northwest Nigeria. These approaches were benchmarked against three established methods—Garika, Hargreaves, and Samani—using monthly meteorological data, including temperature, sunshine duration, and GSR (Olomiyesan et al., 2017). Similarly, Nage (2018) reviewed multiple models based on Ethiopia's sunshine hours and temperature data. In China, Haushan Li et al. proposed a novel model for calculating GSR across 65 locations, grounded in the Hargreaves and Samani (HS) approach (Li et al., 2014). The authors subsequently compared the proposed model against the Chen, Samani, and HS models to evaluate its accuracy and efficiency.

Hassan et al. evaluated the performance of 20 models designed to predict GSR using air temperature as a key parameter. Among these, 17 models were newly formulated, while the remaining three—developed by Allen (1997), Goodin et al. (1999), and Annandale et al. (2002)—had been previously established specifically for estimating GSR in Egypt. (Hassan et al. 2016).

The solar energy capacity of Shenzhen, China, was assessed by Yaning An et al. using GIS-based data about urban residential environments (Yaning An et al., 2023). Similarly, Romero-Ramos, J.A. employed a GIS-AHP methodology to explore the feasibility of utilizing solar energy to fulfil thermal energy demands in the industrial sector of southeastern Spain (Romero-Ramos, J.A. et al., 2023).

Akpootu D.O. and colleagues estimated GSR levels in Maiduguri, Nigeria, utilizing models based on sunshine duration and temperature data (Akpootu D.O. et al., 2023).

Furthermore, K.A. Narejo et al. developed innovative mathematical models for predicting solar radiation in Pakistan, aligning with existing benchmarks. Leveraging these models, they computed three categories of solar radiation—global, beam, and diffuse—for five major cities worldwide, including New York, Tokyo, Karachi, Sydney, and London (K.A. Narejo et al., 2024).

González-Plaza et al. (2024) developed a predictive model for monthly GSR in Spain, leveraging artificial intelligence, temperature data, and geographic variables. In contrast, Joshi et al. (2021) employed a range of established techniques to estimate GSR in Khumaltar, Nepal. Dhakal et al. (2020) investigated several approaches, including conventional mathematical models and advanced machine learning algorithms, to forecast GSR in Biratnagar, Nepal, which rely on temperature data inputs. Additionally, Joshi et al. used RadEst 3.0, a specialized software tool, to determine the daily GSR in Simikot, situated in Nepal's western highlands. (Joshi et al. 2022)

Bristow and Campbell introduced a model to explain the diurnal fluctuations in near-surface air temperature and atmospheric radiation transmissivity. Over the years, this model has been enhanced and applied in numerous studies. A seasonal adjustment factor was incorporated into the model to account for variations in the mid-latitude regions. This concept was then employed in the development of weather generators. (Bristow and Campbell 1984)

Donatelli and Bellocchi (2001) and Donatelli et al. (2003) concentrated on refining techniques to monitor seasonal variations in solar radiation across various locations. Poudyal et al. (2013) utilized the RadEst 3.0 software to estimate the GSR in Kathmandu, Nepal, for the years 2005

and 2007. Similarly, they applied the same methodology to assess GSR at Simara Airport in Nepal (Poudyal et al. 2012). Using data from 2011 and 2013, Chhetri and Gurung estimated the GSR in Jumla, Nepal, employing the RadEst 3.00 program. (Chhetri and Gurung 2017).

This research aims to analyse the spatial distribution of solar energy throughout Nepal, a country abundant in underutilized solar resources. The research employs local meteorological data along with advanced modelling approaches to precisely assess GSR levels. By evaluating various models, the researchers identify the most effective technique for predicting solar radiation in Janakpur. The findings offer crucial insights that can aid in the strategic planning of future solar energy initiatives and support the advancement of sustainable energy development in Nepal.

2. RadEst 3.0 Program

High-quality data from comprehensive radiation observations across all main climatic zones are necessary to determine a region's GSR. Different empirical formulas have been created using different criteria to determine the daily GSR at various sites worldwide. The RadEst 3.0 program is one potential choice that determines the daily GSR using the highest and lowest temperatures.

This article introduces RadEst 3.0 software, which allows the user to determine the daily GSR based on geographical location, maximum and minimum humidity, precipitation, average air speed, and temperature. To support the development of solar power technology in Nepal and to facilitate future research in comparable geographic areas, the primary goal of this study is to identify the optimal model for the link between GSR, temperature, and precipitation. RadEst 3.0 software was selected because of its dependability, ease of use, and versatility, as well as the fact that air temperature, humidity, wind speed, and precipitation are easily accessible from meteorological stations across the globe.

The RadEst 3.00 software was developed as a collaborative effort between ISCI-Crop Science and the FAO-SDRN-Agrometeorology Group. This application uses four fundamental models to estimate the daily global sun radiation at a given location. Both statistical and visual methods can be used to analyze the software's output.

Models

The amount of solar radiation that reaches the Earth's surface each day is estimated using four models. These models were created by Donatelli, Campbell, Bristow, and Bellocchi and are referred to as DCBB, BC, CD, and DB. Based on several input variables, these models compute estimated radiation using statistical techniques. These factors include:

tt_i = estimated atmospheric transmissivity,

 τ = clear sky transmissivity,

 ΔT = average monthly temperature

 $T_{max} = maximum daily air temperature$

 T_{min} = minimum daily air temperature,

Nanotechnology Perceptions Vol. 20 No. S16 (2024)

b = temperature range coefficient

c = highly sensitive empirical parameter,

 T_{nc} = thermal factor

 c_1 = magnitude parameter for seasonal variation

 c_2 = profile coefficient for seasonal variation

i = day number of the year, i = 1 to 365 or 366

 $f(T_{avg}) = average temperature function,$

 $f(T_{min}) = minimum temperature function$

Est Rad_i = estimated radiation (MJ m⁻² day⁻¹)

PotRad_i = Extraterrestrial radiation i.e. radiation beyond Earth's atmosphere (MJ m⁻² day⁻¹)

By examining daily temperature variations, these models calculate the amount of solar radiation that enters the atmosphere. The estimated atmospheric transmissivity (tti) is multiplied by the total potential solar radiation (Pot Radi) at the top of the atmosphere to determine the expected amount of solar radiation (Est Radi) that reaches the Earth's surface.

 $Est Rad_i = tt_i Pot Rad_i$

Pot
$$\operatorname{Red}_{\operatorname{doy}} = 117.5 \operatorname{dd}_2 \frac{\operatorname{h_sSin(lat)} \operatorname{Sin(dec)} + \operatorname{Cos(lat)} \operatorname{Sin(h_s)}}{\pi}$$
 (1)

This equation utilizes the following variables: latitude of the observation point (lat) in degrees, solar declination (dec), the sun's distance (dd2), and half-day duration (h_s).

2.1 Bristow and Campbell Model

Later models were built on top of the original model, which was created by Bristow and Campbell. By analyzing the relationship between daily temperature variations and total solar radiation, this model determines the daily quantity of incoming solar radiation. It assumes that clearer skies (lower transmissivity) are associated with higher daily temperatures, and vice versa.

Both the maximum and minimum temperatures are affected by cloud cover. While clear sky produces colder nights because heat escapes more easily, cloudy conditions result in warmer nighttime temperatures because heat is held by the clouds. On the other hand, because more solar energy reaches the Earth's surface when the sky is clear, daytime temperatures rise. Over time, this technique for calculating solar radiation based on temperature variations has been used extensively and improved.

Estimated atmospheric transmissivity is

$$tt_{i} = \tau \left[1 - \exp\left(\frac{-b\,\Delta T_{i}^{c}}{\mathrm{month}\,\Delta T}\right) \right] \tag{2}$$

Hence from the equation, the estimated radiation provided is given by,

Est
$$\operatorname{Red}_{i} = \tau \left[1 - \exp\left(\frac{-b \Delta T_{i}^{c}}{\operatorname{month} \Delta T}\right) \right] \operatorname{PotRed}_{i}$$
 (3)

Nanotechnology Perceptions Vol. 20 No. S16 (2024)

Where.

$$\Delta T_{i} = T_{\text{max}_{i}} - \frac{T_{\text{min}_{i}} + T_{\text{min}(i+j)}}{2} \tag{4}$$

2.2 Campbell and Donatelli Model

The original Bristow and Campbell (BC) model was improved upon to create the Campbell and Donatelli (CD) model. The CD model includes a correction factor to take into consideration seasonal variations that are typical in mid-latitude areas like Nepal. Especially on summer evenings, this variable, called $T_{\rm nc}$, modifies the expected transmissivity. The model calculates transmissivity as,

$$tt_{i} = \tau \left[1 - \exp\left\{-b \times f\left(T_{avg}\right) \Delta T_{i}^{2} f(T_{min})\right\}\right]$$
(5)

Thus.

Est Red_i =
$$\tau \left[1 - \exp\left\{-b \times f\left(T_{avg}\right) \Delta T_i^2 f_1(T_{min}) \text{ PotRed}_i\right\}\right]$$
 (6)

Where.

$$T_{\text{avg}} = \frac{T_{\text{max}_i} + T_{\text{min}_i}}{2} \tag{7}$$

2.3 Donatelli and Bellocchi Model

Donatelli and Bellocchi created the third model, which uses air temperature to determine total solar energy. In contrast to earlier models, this one takes annual variations in atmospheric clarity into account. The model computes temperature differences using two additional components, c_1 and c_2 , to account for seasonal variations. The model determines transmissivity as,

$$tt_{i} = \tau \left[1 + f(i) \left[1 - \exp\left\{ \frac{-b \Delta T^{2}}{\Delta T_{\text{week}}} \right\} \right] \right]$$
 (8)

Providing radiation estimates as,

$$EstRed_{i} = \tau \left[1 + f(i) \left[1 - exp \left\{ \frac{-b \Delta T_{i}^{2}}{\Delta T_{week}} \right\} \right] \right] PotRed_{i}$$
 (9)

Where.

$$f(i) = c_1 \left[\sin \left(i c_2 \frac{\pi}{180} \right) + \cos \left\{ i f(c_2) \frac{\pi}{180} \right\} \right]$$
 (10)

$$f(c_2) = 1 - 1.90 c_3 + 3.83 c_3^2$$
 (11)

$$c_3 = c_2 \text{ integer } (c_2) \tag{12}$$

2.4 Donatelli-Campbell-Bristow-Bellocchi Model

The fourth model relies on variations in atmospheric air quality. Each of the three versions has features that may be turned on and off. Setting parameter c1 to zero, for instance, simplifies the model. The BC model is equal to the DCBB model under some circumstances, such as when the $T_{\rm nc}$ factor is removed, and average monthly temperature differences are applied. The

estimated transmissivity under these circumstances is,

$$tt_{i} = \tau \left[1 + f(i) \left[1 - \exp\left\{ \frac{-b \Delta T^{2} f(T_{\min})}{\Delta T_{\text{avg}}} \right\} \right] \right]$$
(13)

Which provides radiation estimates as,

 $EstRed_i =$

$$\tau \left[1 + f(i) \left[1 - \exp\left\{ \frac{-b \Delta T_i^2 f(T_{\min})}{\Delta T_{\text{avg}}} \right\} \right] \right] \text{PotRed }_i$$
 (14)

Where.

$$f(i) = c_1 \left[\sin \left(i c_2 \frac{\pi}{180} \right) + \cos \left\{ i f(c_2) \frac{\pi}{180} \right\} \right]$$
 (15)

$$f(c_2) = 1 - 1.90 c_3 + 3.83 c_3^2$$
 (16)

$$f(T_{avg}) = 0.017exp \left\{ exp \left(-0.053 \times T_{avg} \right) \right\}$$
(17)

Where.

$$T_{avg} = \frac{T_{max_i} + T_{min_i}}{2}$$
(18)

$$f(T_{min}) = exp \frac{T_{min}}{T_{nc}}$$
(19)

 $c_3 = c_2$ integer (c_2)

3. Techniques and Instrumentation

3.1 Study Site Determination

Biratnagar, Nepal, located in the southeastern Terai region at 26.45° N, 87.27° E, sits at 72 m. As Nepal's second-largest city and an industrial hub, it borders Bihar, India, to the south and lies in Koshi Province. The city experiences a tropical climate with hot summers ($25 - 40^{\circ}$ C), mild winters ($10 - 20^{\circ}$ C), and moderate spring and autumn temperatures ($20 - 30^{\circ}$ C). The monsoon season brings heavy rainfall from June to September.

3.2 Instrument

Biratnagar received meteorological data for 2020, 2022, and 2023 from the Government of Nepal's Department of Hydrology and Meteorology (DHM/GoN). The models used this data as input, which included wind speed, precipitation, humidity, peak and lowest temperatures, and solar radiation. Temperature is measured by a maximum-minimum thermometer, and rainfall is measured with a udometer. GSR is tested with the Pyranometer CMP6. At the heart of this gadget is a thermocouple. The radiation intensity in w/m2 is directly read into the data recorder. Direct conversion of radiation into a temperature differential causes a voltage

difference to arise. This apparatus can operate in temperatures between -40 and 80 degrees Celsius and detect light in a wide spectrum from 310 to 2800 nanometers.

3.3 File Structure

The input data is saved without column headings in plain text (ASCII) format. Eight space-separated columns of yearly model data (days 1 to 365 or 366 for leap years) are included in each DAT file (compatible with Golden Software Surfer 2019). Rainfall (in mm), temperature (in 0C), GSR (in MJ/m2/day), humidity (in %), and wind speed (in m/s) are all represented by these columns. GSR daily values for 2020, 2022, and 2023 have been computed using input data from Biratnagar, Nepal.

3.4 Input Structure

The latitude, longitude, and altitude of the chosen site must be entered into the RadEst ver. 3.00 software. Values for clear sky transmissivity should be set between 0.6 and 0.8. Estimated radiation is calculated using latitude, and the atmospheric transmissivity coefficient is computed using clear sky transmissivity.

3.5 Analysis

The initial step involves specifying the location, including its latitude, longitude, and altitude. Afterwards, the data file is opened in ASCII (American Standard Code for Information Interchange) format. Various models apply Automatic Optimization (AO) and Parameter Fitting (PF) techniques. For accurate GSR estimation and comparison, a minimum of two years' worth of data is required. The performance of AO is generally lower than PF. To align the estimated solar radiation with the observed data, the parameter fitting procedure is adjusted to match the average values. A visual comparison of estimated versus observed radiation is performed. Statistical metrics, such as MBE, correlation coefficient (r), coefficient of determination (R²), RMSE, MPE, mean error (ME), and coefficient of variation (CV), are used to assess the precision of the predictions. Multiple tools are employed to support the modelling process.

4. Results and discussion

All models were subjected to auto-optimization testing, resulting in estimated GSR values that differed significantly from the measured GSR. The four models were calibrated using parameter fitting (PF) with 2022 Biratnagar data, aiming to maximize the R² while minimizing RMSE and CRM. Table 2 compares the measured and model-estimated average, peak, and total annual GSR values for both auto-optimization and parameter fitting in Biratnagar for 2022. The average annual GSR was found to be 15.4 MJ/m²/day. Among the models, the DCBB model provided the closest approximation. It excelled over the other models in predicting the total GSR for 2022. The measured total solar radiation of 5634 MJ/m² closely aligns with the DCBB model's PF estimate of 5212 MJ/m², highlighting its greater accuracy in GSR estimation for 2022.

The GSR for 2020 and 2022 was estimated using the calibrated parameter values from 2023. The measured and estimated GSR values showed strong alignment. Tables 1 and 3 display the

results of the parameter fitting tests for 2023 and 2020. The DCBB model demonstrated performance on par with the other three models in terms of maximum, average, and total annual GSR values across the three years (2020, 2022, and 2023). As a result, the DCBB model is considered the most reliable for estimating GSR in low-altitude areas during this period.

Table 1 The measured and model-estimated average, maximum, and annual total values of GSR at Biratnagar for 2023.

Model	Average GSR (MJ/m ² /day)			Maximum GSR (MJ/m² /day)			Total GSR (MJ/m ²)		
	AO	Mea	PF	AO	Mea	PF	AO	Mea	PF
ВС	15.3	14.8	14.8	26.2	27.3	26.0	5570	5397	5417
CD	17.5	14.8	14.8	28.1	27.3	27.1	6392	5397	5393
DB	14.8	14.8	14.8	23.5	27.3	23.5	5387	5397	5387
DCBB	17.3	14.8	14.8	26.7	27.3	25.0	6302	5397	5401

Table 2 The measured and model-estimated average, maximum, and annual total values of GSR at Biratnagar for 2022

Model	Average	GSR (MJ/n	n² /day)	Maximun	Maximum GSR (MJ/m² /day)			Total GSR (MJ/m ²)		
	AO	Mea	PF	AO	Mea	PF	AO	Mea	PF	
BC	15.8	15.4	14.4	24.8	29.6	23.9	5749	5634	5241	
CD	16.5	15.4	13.9	26.0	29.6	24.8	6032	5634	5061	
DB	15.2	15.4	14.2	22.8	29.6	22.4	5562	5634	5192	
DCBB	15.5	15.4	14.3	26.4	29.6	24.0	5667	5634	5212	

Table 3 The measured and model-estimated average, maximum, and annual total values of GSR at Biratnagar for 2020.

	<u> </u>								
Model	Average GSR (MJ/m²/day)		Maximum GSR (MJ/m²/day)			Total GSR (MJ/m ²)			
	AO	Mea	PF	AO	Mea	PF	AO	Mea	PF
BC	14.9	14.7	14.5	25.7	27.2	25.3	5454	5355	5302
CD	16.3	14.7	14.1	26.6	27.2	25.1	5941	5355	5164
DB	14.4	14.7	14.4	22.4	27.2	22.8	5271	5355	5259
DCBB	14.7	14.7	14.4	24.6	27.2	23.9	5369	5355	5253

4.1 Error analysis

Tables 4, 5, and 6 present a statistical comparison of measured and estimated GSR for 2023, 2022, and 2020, respectively. The correlation and determination coefficients indicate a moderate relationship between the measured and estimated values in all three years. The R² values for the DCBB model were 0.63, 0.63, and 0.65 for 2020, 2022, and 2023, respectively, which are higher than those of all other models, signifying greater consistency. Additionally, 2022 demonstrated better consistency than 2020 and 2023 across all models. Furthermore, for the DCBB model in all three years, the RMSE, MBE, MPE, and CRM values were lower

compared to the other three models. This suggests that the modular DCBB model outperforms the others, likely due to local weather conditions and rainfall patterns.

Error Analysis

Table 4 Statistical Error for the year 2023 for Biratnagar

Model	MBE	RMSE	MPE	r	CRM	\mathbb{R}^2	ME	CV
	(MJ/m²/day)	(MJ/m²/day)	(%)		(MJ/m²/day)			
BC	0.05454	3.79	-11.941	0.7498	0.00	0.56	0.55	25.61
CD	-0.0089	3.67	-9.2052	0.7822	0.00	0.61	0.58	24.81
DB	-0.0268	3.75	-13.222	0.74882	0.00	0.56	0.56	25.38
DCBB	0.01304	3.33	-11.533	0.80844	0.00	0.65	0.65	22.53

Table 5 Statistical Error for the year 2022 for Biratnagar

Model	MBE	RMSE	MPE	r	CRM	\mathbb{R}^2	ME	CV
	(MJ/m²/day)	(MJ/m²/day)	(%)		(MJ/m ² /day)			
ВС	-1.075	3.41	2.7833	0.73526	0.07	0.54	0.48	22.12
CD	-1.568	3.41	7.70326	0.78049	0.10	0.61	0.48	22.12
DB	-1.2091	3.49	2.7418	0.72051	0.08	0.52	0.45	22.59
DCBB	-1.1553	3.12	3.67094	0.79068	0.07	0.63	0.56	20.18

Table 6 Statistical Error for the year 2020 for Biratnagar

Model	MBE	RMSE	MPE	r	CRM	\mathbb{R}^2	ME	CV
	(MJ/m ² /day)	(MJ/m²/day)	(%)		(MJ/m²/day)			
BC	-0.14515	3.70	-10.0965	0.76919	0.01	0.59	0.58	25.23
CD	-0.522282	3.55	-5.70777	0.79591	0.04	0.63	0.62	24.21
DB	-0.26245	3.72	-11.2318	0.76225	0.02	0.58	0.58	25.37
DCBB	-0.27836	3.48	-9.54355	0.79631	0.02	0.63	0.63	23.72

Figures 1, 2, and 3 depict the daily variations in measured and estimated GSR for four models in 2023, 2022, and 2020, respectively. The close alignment between estimated and observed daily GSR values across different models is noteworthy.

Figures 4a, 4b, and 4c display the transmission coefficient for 2023, 2022, and 2020, respectively. Figures 5a, b, and c show the daily variations in observed, potential, and transmitted radiation, highlighting the abundant GSR in the study area. The low altitude of Biratnagar during winter results in a lower solar angle, which reduces radiation levels but increases atmospheric transparency. During the summer months (June, July, and August), increased rainfall, cloud cover, and wind speeds lead to substantially lower GSR levels compared to other seasons, despite the hot weather. However, the rainfall helps clear the sky, leading to a higher radiation flux in the autumn.

In 2020, rainfall was higher (2580.1 mm) compared to 2022 (1816.48 mm) and 2023 (1646.5 mm). The combination of elevated temperatures and rainfall during the summer months results in reduced GSR. Overall, GSR rises steadily from June to August before gradually declining *Nanotechnology Perceptions* Vol. 20 No. S16 (2024)

through to December. However, this trend fluctuates due to the influence of temperature and precipitation. During June, July, and August, the GSR is lower due to rainfall and cloudy skies. GSR shows a positive correlation with temperature and a negative correlation with precipitation.

Table 7 presents the seasonal GSR for 2020, 2022, and 2023, along with their respective standard errors. Table 8 displays the monthly GSR for the same years, with corresponding standard errors. Table 9 provides the seasonal average mean wind speed and seasonal rainfall data for 2020, 2022, and 2023.

Table 7 Seasonal GSR with error

Seasons	GSR 2020	GSR 2022	GSR 2023
winter	$10.8035116 \pm 0.35617143$	11.52572 ± 0.33169528	$10.0514901 \pm 0.29874379$
spring	$18.7385348 \pm 0.52925158$	18.4328633 ± 0.37288221	$18.9838252 \pm 0.52656165$
summer	15.677233 ± 0.6080151	16.5969874 ± 0.55546232	16.098103 ± 0.6261608
autumn	13.3829235 ± 0.54132119	15.0951455 ± 0.37339456	13.893091 ± 0.4242925

Table 8 Monthly GSR with error

Months	GSR (in MJ/m²/ day)								
	2020	2022	2023						
January	8.76027484 ± 0.53972137	9.7976129 ± 0.4422573	9.51281806 ± 0.31689777						
February	13.3720841 ± 0.56103679	$13.9995343 \pm 0.61331718$	12.39468 ± 0.39902652						
March	18.5242181 ± 0.79352377	$17.2217297 \pm 0.50638733$	$15.8521858 \pm 0.84702864$						
April	19.238384 ± 0.86331734	18.569796 ± 0.68695639	19.225848 ± 0.78904563						
May	18.4691265 ± 1.08749443	$19.5114813 \pm 0.68227335$	21.881249 ± 0.76647607						
June	15.775844 ± 1.24867016	14.199544 ± 0.87345727	19.498944 ± 0.93026136						
July	$14.0320452 \pm 0.93631877$	$18.2372013 \pm 0.79727068$	$15.7726645 \pm 0.98877668$						
August	17.226991 ± 0.90667698	17.27688 ± 1.06661355	13.1324052 ± 1.03561879						
September	11.251204 ± 1.14439878	14.343352 ± 0.82801946	15.410308 ± 0.98881674						
October	15.4853613 ± 0.71618684	16.36872 ± 0.65556796	$13.4473006 \pm 0.59945506$						
November	13.342124 ± 0.76570699	14.530912 ± 0.28145478	12.836524 ± 0.45592734						
December	10.4438903 ± 0.4492703	$11.0194142 \pm 0.39228545$	$8.48237419 \pm 0.53082257$						

Table 9 Rainfall and Average wind-speed

Seasons	Average Mean Speed (m/s)			Rainfall (mm	Rainfall (mm)			
	2020	2022	2023	2020	2022	2023		
winter	0.98055385	1.81042222	1.56941333	24.2	18.71	0		
spring	2.02471304	3.341	2.81949239	287.7	186.93	137.43		
summer	2.00124783	3.10347717	2.83765496	1681.7	1050.41	1232.46		
autumn	0.83353503	1.64818901	1.542	586.5	560.43	276.61		

Figure 6 depicts the seasonal variation in GSR for the years 2023, 2022, and 2020. The highest GSR values are observed in spring (18.74 \pm 0.53 MJ/m²/day, 18.43 \pm 0.37 MJ/m²/day, and 18.98 \pm 0.53 MJ/m²/day for 2020, 2022, and 2023, respectively), attributed to clear skies following the monsoon season. In contrast, the lowest GSR values occur in winter (10.80 \pm 0.36 MJ/m²/day, 11.53 \pm 0.33 MJ/m²/day, and 10.05 \pm 0.30 MJ/m²/day for 2020, 2022, and 2023, respectively) due to cloud cover and rainfall.

Solar radiation was highest in spring and lowest in winter across all three years. Spring GSR levels surpassed those of summer and autumn, likely due to lower humidity, reduced cloud cover, minimal rainfall, and less wind. After the monsoon rains in June, July, and August, clear skies contributed to the peak radiation levels.

Figure 7 illustrates the monthly variations in GSR for the years 2023, 2022, and 2020. The highest GSR values were recorded in May 2023 (21.88 \pm 0.77 MJ/m²/day), May 2022 (19.51 \pm 0.68 MJ/m²/day), and April 2020 (19.24 \pm 0.86 MJ/m²/day), likely due to clear skies following the monsoon rains. On the other hand, the lowest GSR values occurred in December 2023 (8.48 \pm 0.53 MJ/m²/day), January 2022 (9.80 \pm 0.44 MJ/m²/day), and January 2020 (8.76 \pm 0.54 MJ/m²/day), primarily due to cloudy skies and rainfall. The overall trend in GSR remained similar across the three years. Error bars, representing the standard deviation, reflect the variability of GSR within each month.

Figure 8 shows the seasonal variation in precipitation for 2023, 2022, and 2020. The highest rainfall was recorded during the summer of 2020 (1681.7 mm), while the lowest occurred in the winter of 2023 (0.00 mm) across the three years. Similarly, Figure 9 illustrates the seasonal changes in average wind speed for 2023, 2022, and 2020. The maximum and minimum average wind speeds were observed in spring (3.34 m/s) for 2022 and autumn (0.83 m/s) for 2020, respectively, over the three years.

The days with the highest solar radiation for the year occurred on June 2 (26.74 MJ/m²/day) in 2020, April 25 (29.56 MJ/m²/day) in 2022, and May 29 (27.29 MJ/m²/day) in 2023. The lowest solar radiation levels were recorded on November 19, 2020 (0.93 MJ/m²/day), June 28, 2022 (1.69 MJ/m²/day), and December 7, 2023 (1.25 MJ/m²/day). The hottest days of the year were August 4 (35.5°C) in 2020, April 15 (38.5°C) in 2022, and June 8 (41.5°C) in 2023. The coldest days were January 2 (5.2°C) in 2020, December 28 (7.1°C) in 2022, and January 14 (6°C) in 2023. The highest rainfall days occurred on September 24 (125 mm) in 2020, August 2 (114.3 mm) in 2022, and August 8 (112.3 mm) in 2023. The days with the highest wind speeds were March 4 (9.86 m/s) in 2020, August 20 (7.50 m/s) in 2022, and June 26 (5.76 m/s) in 2023.

The Simikot region, located at a higher altitude in the mountains, receives lower GSR compared to the mid-hill region of Jumla. In 2013, the GSR in Simikot was 6648 MJ/m²/day, and in 2011, it was 7309 MJ/m²/day. The BC model proves to be more effective in estimating GSR in Jumla than in Simikot. While Simikot experiences higher GSR during spring and autumn, Jumla's peak GSR occurs in the spring. These differences are primarily attributed to local weather conditions and altitude variations (Chhetri and Gurung 2017).

Despite Simikot's higher altitude, Jumla receives more solar radiation. This is probably because of factors like clearer skies and less cloud cover in Jumla, allowing more sunlight to

reach the ground directly. Seasonal variations, particularly during spring when the sun is positioned more directly overhead, may also contribute to Jumla's higher GSR. Additionally, the specific locations and methods used for measurements could influence the recorded data, highlighting that solar radiation patterns can vary significantly between different regions.

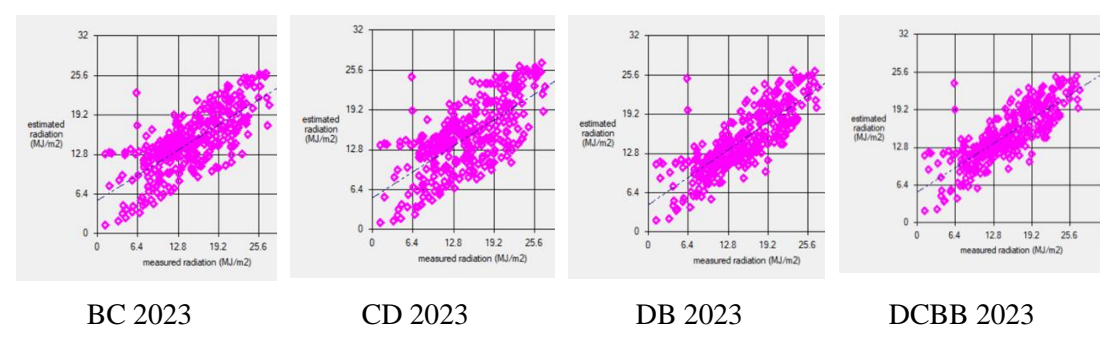


Fig. 1 Linear relationship analysis of measured and estimated GSR data for Biratnagar in 2023.

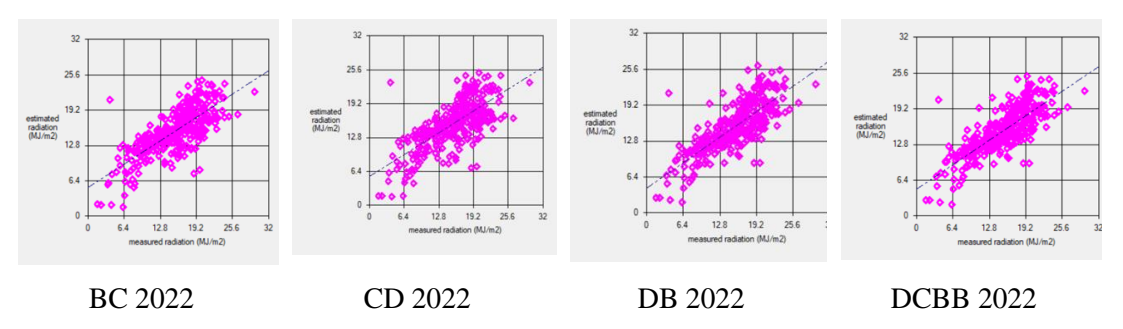


Fig. 2 Linear relationship analysis of measured and estimated GSR data for Biratnagar in 2022

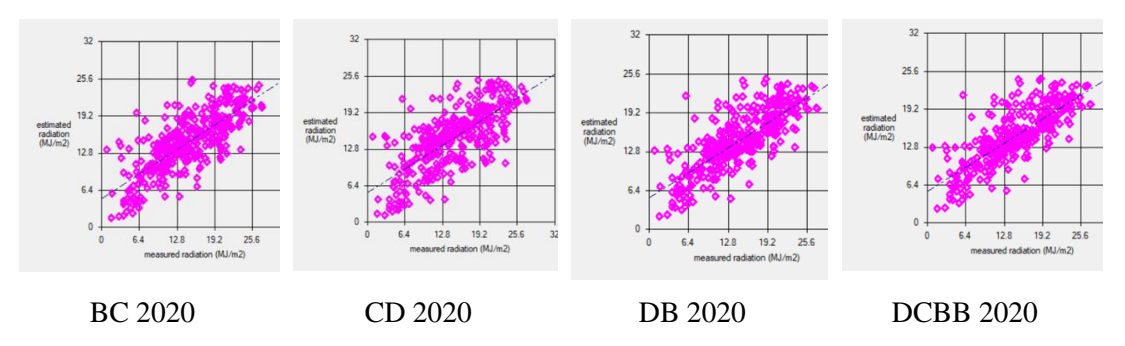
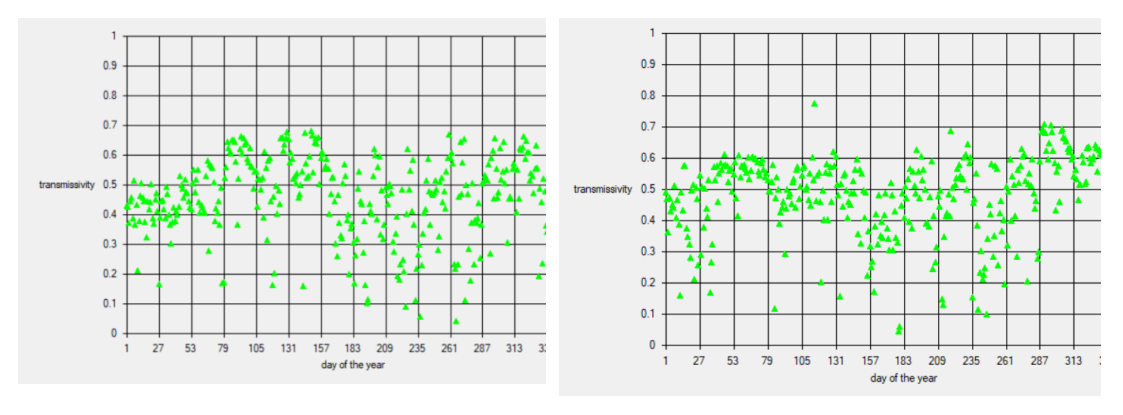
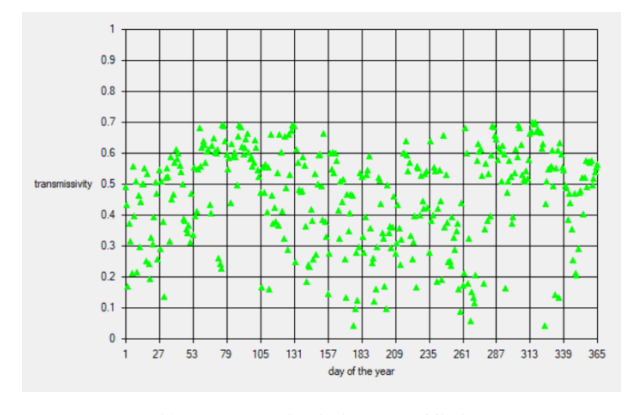


Fig. 3 Linear relationship analysis of measured and estimated GSR data for Biratnagar in 2020

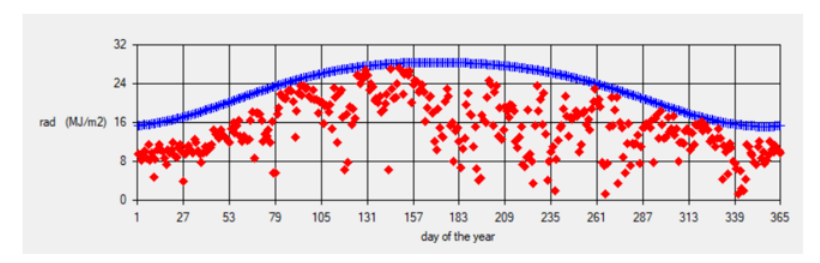


- 4 a. Daily Transmissivity coefficient 2023
- 4 b. Daily Transmissivity coefficient 2022

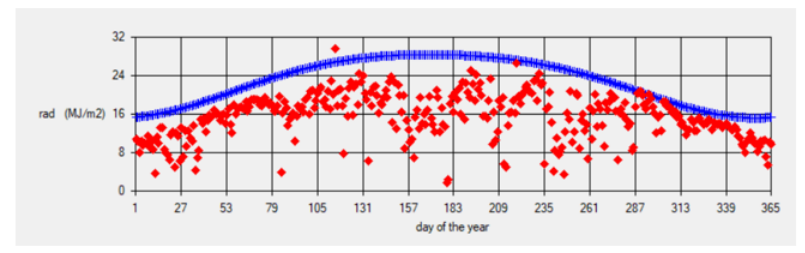


4 c. Daily Transmissivity coefficient 2020

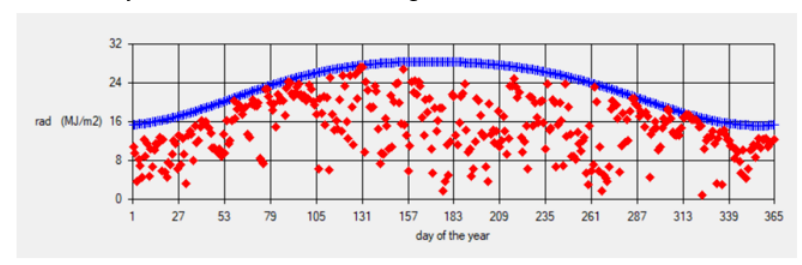
Fig. 4 Fluctuations in the daily transmissivity coefficient for Biratnagar during 2023, 2022, and 2020



a. Daily fluctuations in GSR at Biratnagar for 2023

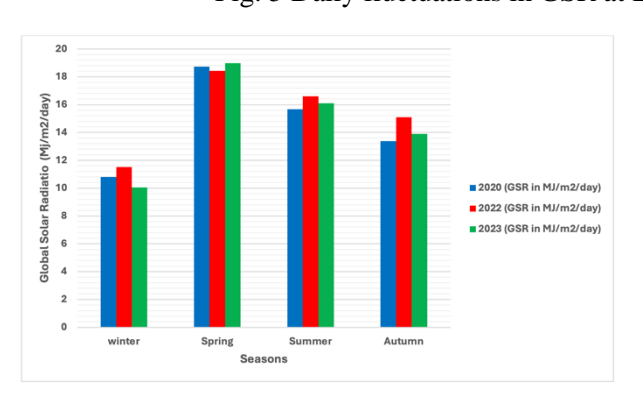


b. Daily fluctuations in GSR at Biratnagar for 2022



c. Daily fluctuations in GSR at Biratnagar for 2020

Fig. 5 Daily fluctuations in GSR at Biratnagar for 2023, 2022, and 2020



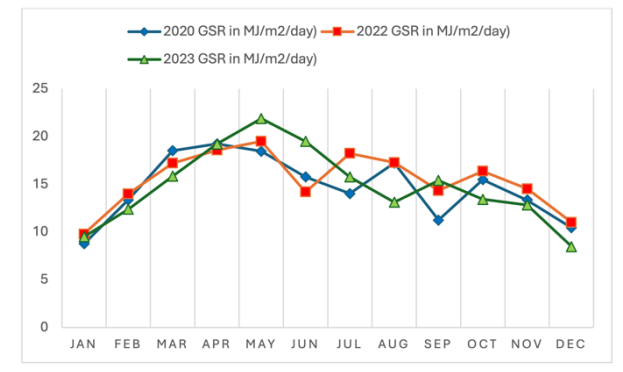
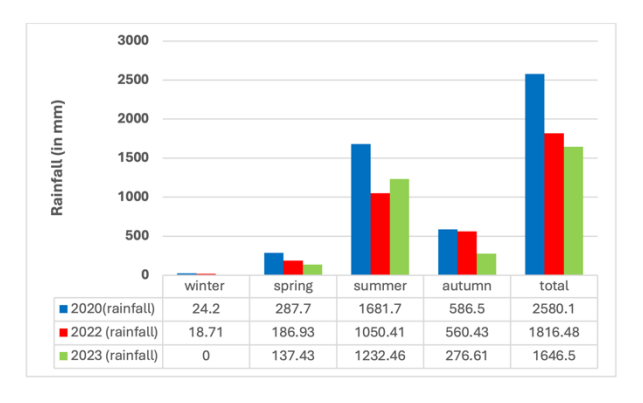


Fig. 6 Seasonal Fluctuation of GSR at Biratnagar

Fig. 7 Monthly Fluctuation of GSR at Biratnagar



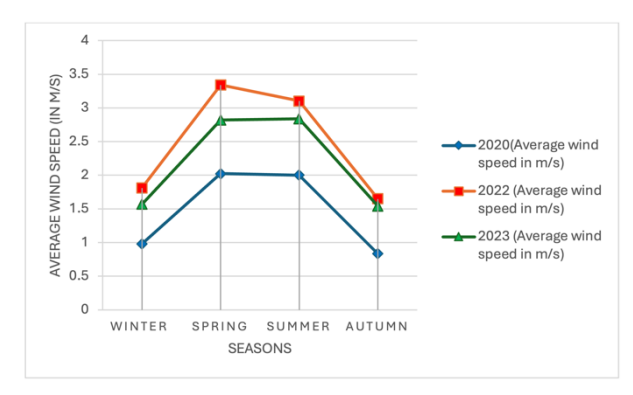


Fig. 8 Seasonal Fluctuation of Precipitation at Biratnagar

Fig. 9 Seasonal Fluctuation of average wind speed at Biratnagar

5. Conclusions

In 2020, 2022, and 2023, the annual average GSR values were 14.7 ± 0.30 MJ/m²/day, 15.4 ± 0.25 MJ/m²/day, and 14.8 ± 0.30 MJ/m²/day, respectively. The highest GSR values recorded in those years were 27.3 MJ/m²/day in 2020, 29.6 MJ/m²/day in 2022, and 27.2 MJ/m²/day in 2023. These figures highlight the substantial solar energy potential in the region, making it ideal for both grid-connected and off-grid power plants, particularly in an area currently experiencing energy shortages. Solar radiation intensity varies due to factors such as temperature, humidity, rainfall, wind speed, and sunlight duration, which all influence the fluctuations in solar energy over time and across different locations.

Because of ground albedo, solar radiation increases after the monsoon season on clear sky days. As a result, topography and local weather conditions play a crucial role in estimating GSR in various locations. In summary, Biratnagar receives an average solar insolation of 4.28 \pm 0.07 kWh/m²/day, indicating considerable potential for rapid development of solar energy. The favorable combination of low air pollution, minimal precipitation, limited cloud cover, reduced humidity, and south-facing mountainous terrain creates optimal conditions for high solar insolation.

In our research analysis, RadEst 3.0 is employed to assess four models. The DCBB model is found to be the most suitable for this high-altitude region, as it exhibits the highest coefficient of determination and fewer errors compared to the other models. In conclusion, the empirical coefficients from the DCBB model can be effectively applied to predict solar radiation and energy potential in similar geographical areas of Nepal.

Acknowledgement

The authors sincerely thank the FAOSDRN Agrometeorology Group in Rome and ISCI-Crop Science in Bologna for providing free access to the RadEst 3.0 software and its documentation for educational purposes. They also acknowledge the DHM/ GoN for providing the necessary meteorological data. Additionally, the authors extend their gratitude to all individuals who contributed to this study.

Nanotechnology Perceptions Vol. 20 No. S16 (2024)

Funding: This research was carried out independently, with no external financial support.

Declarations: The authors confirm that they have no conflicts of interest.

References

- 1. An, Y., Chen, T., Shi, L., Heng, C. K., & Fan, J. (2023). Solar energy potential using GIS-based urban residential environmental data: A case study of Shenzhen, China. Sustainable Cities and Society, 93, 104547.
- 2. Akpootu, D. O., Alaiyemola, S. R., Abdulsalam, M. K., Bello, G., Umar, M., Aruna, S., ... & Badmus, T. O. (2023). Sunshine and temperature-based models for estimating global solar radiation in Maiduguri, Nigeria. Saudi Journal of Engineering and Technology, 8(5), 82-90.
- 3. Allen RG (1997) Self-calibrating method for estimating solar radiation from air temperature. J Hydrol Eng 2(2):56–67
- 4. An, Y., Chen, T., Shi, L., Heng, C. K., & Fan, J. (2023). Solar energy potential using GIS-based urban residential environmental data: A case study of Shenzhen, China. Sustainable Cities and Society, 93, 104547.
- 5. Angstrom A (1924) Solar and terrestrial radiation. Report to the International Commission for Solar Research on actinometric investigations of solar and atmospheric radiation. Quarterly J Royal Meteorol Soc 50(210):121–126
- 6. Annandale J, Jovanovic N, Benade N, Allen R (2002) Software for missing data error analysis of penman-monteith reference evapotranspiration. Irrig Sci 21(2):57–67
- 7. Bristow KL, Campbell GS (1984) On the relationship between incoming solar radiation and daily maximum and minimum temperature. Agric for Meteorol 31(2):159–166
- 8. Chhetri BRK, Gurung S (2017) Estimation of total solar radiation using Radest 3.00 software at Jumla, Nepal. Int J Syst Assur Eng Manag 8(2):1527–1533
- 9. Dhakal S, Gautam Y, Bhattarai A (2020) Evaluation of temperature-based empirical models and machine learning techniques to estimate daily global solar radiation at Biratnagar Airport Nepal. Adv Meteorol 2020:1–11
- 10. Donatelli M, Bellocchi G, (2001) Estimate of daily global solar radiation: new developments in the software radest3.00. In: Proceedings of the 2nd international symposium modeling cropping systems, Inst. for Biometeorology CNR, Florence, Italy, 213–214
- 11. Donatelli M, Bellocchi G, Fontana F (2003) Radest3.00: software to estimate daily radiation data from commonly available meteorological variables. Eur J Agron 18(3–4):363–367
- 12. Donatelli, M. Campbell, G.S. 1998, "A simple model to estimate global solar radiation", Proceedings of the 3rd Congress of the Europe Society for Agronomy, Nitra, Slovakia, II, pp. 133–134.
- 13. Golden Software/Surfer. Surfer 13. [Online; accessed 26-March- 2019]
- 14. González-Plaza, E., García, D., & Prieto, J. I. (2024). Monthly Global Solar Radiation Model Based on Artificial Neural Network, Temperature Data and Geographical and Topographical Parameters: A Case Study in Spain. Sustainability, 16(3), 1293.
- 15. Goodin DG, Hutchinson J, Vanderlip RL, Knapp M (1999) Estimating solar irradiance for crop modeling using daily air temperature data. Agron J 91(5):845–851
- 16. Hassan GE, Youssef ME, Mohamed ZE, Ali MA, Hanafy AA (2016) New temperature-based models for predicting global solar radiation. Appl Energy 179:437–450
- 17. Iqbal M (1983) An introduction to solar radiation. Academic Press, New York, NY
- 18. Joshi U, Karki IB, Chapagain NP, Poudyal KN (2021) Prediction of daily global solar radiation using different empirical models based on meteorological parameters at Trans Himalaya Region. Nepal BIBECHANA 18(1):159–169
- 19. Joshi U, Poudyal KN, Karki IB, Chapagain NP (2020) Evaluation of global solar radiation using

- sunshine hour, temperature and relative humidity at low land region of Nepal. J Nepal Phys Soc 6(1):16-24
- 20. Joshi, U., Chapagain, N. P., Karki, I. B., Shrestha, P. M., & Poudyal, K. N. (2022). Estimation of daily solar radiation flux at Western Highland, Simikot, Nepal using RadEst 3.0 software. International Journal of System Assurance Engineering and Management, 13(1), 318-327.
- 21. Kudish A, Wolf D, Machlav Y (1983) Solar radiation data for beer Sheva. Israel Solar Energy 30(1):33–37
- 22. Lamsal H (2019) Nea to connect all households with electricity by 2022. Republica
- 23. Li H, Cao F, Wang X, Ma W (2014) A temperature-based model for estimating monthly average daily global solar radiation in China. Sci World J 2014:1–9
- 24. Nage GD (2018) Estimation of monthly average daily solar radiation from meteorological parameters: sunshine hours and measured temperature in Tepi, Ethiopia. Int J Energy Environ Sci 3(1):19–26
- 25. Narejo, K. A., Rehman, S. U., Tariq, I., Zahid, M. M., Sadiq, N., Khan, M. M., & Uddin, Z. (2024). MEP modelled new equations for ASHRAE constant to estimate solar radiation. Indian Journal of Physics, 1-5.
- 26. Olomiyesan B, Oyedum O, Ugwuoke P, Abolarin M (2017) Evaluation of some global solar radiation models in selected locations in northwest, Nigeria. Open Access J Photo Energy 1(1):1–6
- Poudyal K N (2015) Estimation of global solar radiation potential in Nepal. Ph D Thesis, IOE, Tribhuvan University
- 28. Poudyal KN, Bhattarai BK, Sapkota B, Kjeldstad B (2012) Estimation of the daily global solar radiation using RadEst 3.00 software-a case study at low land plain region of Nepal. J Nepal Chem Soc 29:48–57
- 29. Poudyal KN, Bhattarai BK, Sapkota B, Kjeldstad B, Daponte P (2013) Estimation of the daily global solar radiation; Nepal experience. Measurement 46(6):1807–1817
- 30. Radest 3.00 version. [Online; accessed 26-March-2019]
- 31. Radiation in central European lowlands is estimated by various empirical formulae. A` gric For Meteorol 131(1–2):54–76
- 32. Research Centre for Industrial Crops Agriculture Research Council.
- 33. Romero-Ramos, J. A., Gil, J. D., Cardemil, J. M., Escobar, R. A., Arias, I., & Pérez-García, M. (2023). A GIS-AHP approach for determining the potential of solar energy to meet the thermal demand in southeastern Spain productive enclaves. Renewable and Sustainable Energy Reviews, 176, 113205.
- 34. Shrestha JN, Bajracharya T, Shakya S, Giri B (2003) Renewable energy in Nepal-progress at a glance from 1998 to 2003. In: proceedings of the international conference on renewable energy technology for rural development (RETRUD-03), pages 12–14
- 35. Team, GEAW et al. (2012). Global energy assessment. Cambridge Books
- 36. WECS, Energy Synopsis Report, 2023, Government of Nepal